ACS OMEGA

http://pubs.acs.org/journal/acsodf

Article

WS_2/Polyethylene Glycol Nanostructures for Ultra-Efficient MCF-7 Cancer Cell Ablation and Electrothermal Therapy

Maria Prisca Meivita, Sophia S. Y. Chan, Shao Xiang Go, Denise Lee, Natasa Bajalovic,* and Desmond K. Loke*

Cite This: *ACS Omega* 2022, 7, 23075−23082

Read Online

ACCESS | Metrics & More | Article Recommendations | Supporting Information

ABSTRACT: Developing novel nanostructures and advanced nanotechnologies for cancer treatment has attracted ever-increasing interest. Electrothermal therapy offers many advantages such as high efficiency and minimal invasiveness, but finding a balance between increasing stability of the nanostructure state and, at the same time, enhancing the nanostructure biodegradability presents a key challenge. Here, we modulate the biodegradation process of two-dimensional-material-based nanostructures by using polyethylene glycol (PEG) via nanostructure disrupt-and-release effects. We then demonstrate the development of a previously unreported alternating current (AC) pulse WS_2/PEG nanostructure system for enhancing therapeutic performance. A decrease in cell viability of ∼42% for MCF-7 cells with WS_2/PEG was achieved, which is above an average of ∼25% for current electrothermal-based therapeutic methods using similar energy densities, as well as degradation time of the WS_2 of ∼1 week, below an average of ∼3.5 weeks for state-of-the-art nanostructure-based systems in physiological media. Moreover, the incubation time of MCF-7 cells with WS_2/PEG reached ∼24 h, which is above the average of ∼4.5 h for current electrothermal-based therapeutic methods and with the use of the amount of time harnessed to incubate the cells with nanostructures before applying a stimulus as a measure of incubation time. Material characterizations further disclose the degradation of WS_2 and the grafting of PEG on WS_2 surfaces. These WS_2-based systems offer strong therapeutic performance and, simultaneously, maintain excellent biodegradability/biocompatibility, thus providing a promising route for the ablation of cancer.

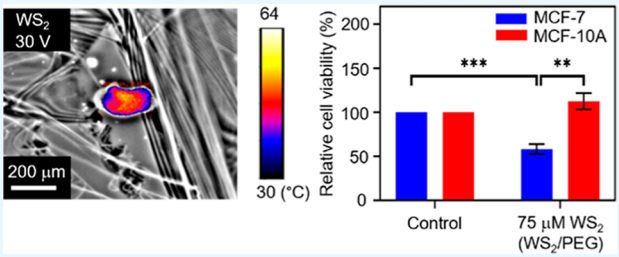

1. INTRODUCTION

Cancer is a leading cause of death worldwide.[1] According to the World Health Organization, cancer accounted for ∼10 million deaths in 2020. In terms of new cases, the number of cases occurring in 2020 was ∼19.3 million, which is expected to increase by ∼47% (∼28.4 million) in 2040.[2] Additionally, approximately one in six patients with cancer who survived Covid-19 developed other side effects from the virus that lingered months later.[3] Thus, developing novel nanostructures and advanced nanotechnologies for cancer treatment has attracted ever-increasing interest. Electrothermal therapy (ETT) is a promising candidate for developing next-generation cancer treatments. ETT operations, based on the localized Joule heating of cancerous cells, ablating tumors without affecting surrounding tissues, offer high efficiency and minimal invasiveness.[4] Because of their excellent thermal performance, nanostructures such as conducting polymer nanoparticles, black phosphorus nanodots, carbon nanotubes, and other nanostructures have been used as thermal agents in cancer therapy.[5−7] Nanostructures with sizes in the 5−500 nm range have long blood circulation time and passively accumulate in tumors for an extended period through enhanced permeability and retention effects.[8] However, conventional inorganic nanostructures may also have poor biodegradability and stay in the body for a long time, increasing the risk of deleterious effects. A difficulty arises from finding a balance between increasing the stability of the nanostructure state for enhancing treatment efficacy and, at the same time, improving the biodegradability/biocompatibility for improving safety.

Two-dimensional (2D) atomically thin tungsten disulfide (WS_2) is a leading contender for next-generation electrothermal agents.[9−11] WS_2 exhibits excellent electrical conductivity and is attractive for a wide range of applications such as electronics and optoelectronics.[12] Moreover, WS_2 has a large band gap ranging from 1.32 eV for bulk materials to 2.03 eV for monolayered WS_2,[13] allowing excellent absorption across the ultraviolet and infrared regions. The liquid-phase exfoliation method is a popular strategy to fabricate WS_2 nanosheets with specified thicknesses and sizes for bioimaging and phototherapy.[9,14,15]

Received: January 14, 2022
Accepted: May 19, 2022
Published: June 27, 2022

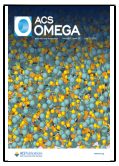

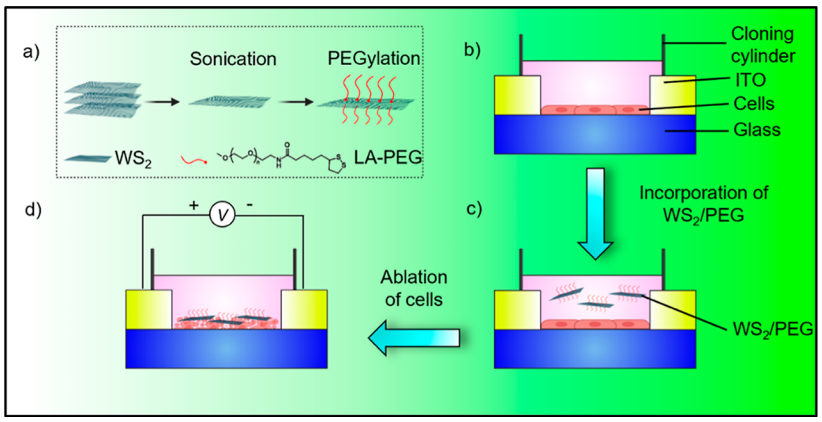

Figure 1. Fabrication of the AC-pulse electrothermal framework based on WS_2/PEG nanostructures. Schematic illustration of the strategy utilized to ablate cancer cells: (a) synthesis of WS_2/PEG, (b) seeding of MCF-7 or MCF-10A cells (~2 × 10^3 cells) in an ITO-on-glass substrate, (c) incorporation of WS_2/PEG into the system, and (d) application of AC pulses in the setup.

For example, experiments have shown that ~5 nm-thick WS_2 nanosheets possess a strong (near-infrared) NIR absorption and thermal conversion and are less cytotoxic.[9] However, clinical adoption of WS_2 nanosheets has been limited by poor stability of the nanosheet state in some solutions due to poor dispersion in aqueous media.

Herein, we show that by altering the biodegradation process, we can alter the stability of the nanostructure state by a polyethylene glycol (PEG)-driven approach to achieve excellent stability of the nanostructure state and, at the same time, maintain good biodegradability. We then demonstrate the development of a previously unconsidered alternating current (AC)-pulse WS_2/PEG nanostructure system for achieving enhanced cancer cell ablation and electrothermal performance (Figure 1). A decrease in cell viability of ~42% for MCF-7 cells with WS_2/PEG and a degradation time of WS_2 of ~1 week were achieved. the incubation time of MCF-7 cells with WS_2/PEG further reached ~24 h. Material characterizations reveal the degradation of WS_2 and the grafting of PEG on WS_2 surfaces. This proposed methodology based on WS_2/PEG nanostructures holds intriguing potential for the development of next-generation cancer treatment platforms, which can be further applied for clinical purposes.

PEG, a well-known biodegradable and biocompatible polymer, is widely utilized as a vehicle in the delivery of drugs and nanostructures.[16] Additionally, PEG shows excellent stability of the polymer state in aqueous media, and the biodegradability of PEG can be controlled by altering its chemical compositions.[17] In previous studies, LA-PEG (lipoic acid-conjugated PEG) was successfully grafted onto the WS_2 surface.[14] This is due to the two sulfur atoms in the LA unit which form a strong bond with the transition metal dichalcogenides (TMDs), allowing the PEG to be assembled on TMDs.[18]

2. MATERIALS AND METHODS

2.1. Material Characterization. The WS_2 in deionized (DI) water was utilized as purchased (2D semiconductors). The solution was bath-sonicated (Elmasonic P) for 25 min to obtain the WS_2 nanosheet samples. These samples were drop-cast on the silicon substrates. The material properties of the WS_2 samples were then evaluated using the atomic force microscopy (AFM) (Bruker Contour GT-K), Raman spectroscopy (HORIBA LabRAM HR 800), lock-in IR thermography (ELITE system), Fourier-transform infrared (FTIR) spectroscopy (PerkinElmer Inc. Spectrum Spotlight 200), and X-ray photoelectron spectroscopy (XPS) in a vacuum chamber (Thermo Fisher 250Xi).

2.2. Synthesis of WS_2/PEG. The as-prepared WS_2 solution (2 mL, concentration = 92 mg/L) was mixed with 0.45 mg of 5 kDa LA-PEG (Nanocs). The mixture was then ultrasonicated for 30 min and stirred overnight. The WS_2/PEG/precipitate was obtained by centrifugation at 14,000 rpm for 10 min and washed with DI water three times. Finally, WS_2/PEG was re-dispersed in DI water and stored at 4 °C.

2.3. Cell Culture. Breast cancer cells (MCF-7) were cultured in Dulbecco's modified Eagle's medium (DMEM) with L-glutamine (Nacalai Tesque) and 7% fetal bovine serum (FBS) (Gibco). Non-malignant breast epithelial cells (MCF-10A) were cultured in DMEM/nutrient mixture F-12 (DMEM/F12) supplemented with 10% FBS, 0.5 μg/mL hydrocortisone, 20 ng/mL epidermal growth factor (Gibco), and 10 μg/mL insulin (Sigma). Both cell lines were maintained at 37 °C under a 5% CO_2 atmosphere.

2.4. In Vitro Cytotoxicity Study. Cells were plated into 96-well plates and cultured for 24 h before treatment with different WS_2 or WS_2/PEG concentrations. Relative cell viabilities were determined using the crystal violet (CV) assay for 24 h after incubation with the material. The CV was prepared by dissolving the powder in methanol (0.05% concentration). The samples, that is, cells with pure WS_2 or WS_2/PEG, were washed using DPBS. The CV was then added to these samples, and the samples were dried overnight at room temperature. The absorbance values of the samples were determined at λ = 570 nm using a multiplate reader (Thermo Scientific Multiskan GO).

2.5. Electrothermal Simulations. The thermal distribution of cell systems was computed using the finite element method (Ansys). Standard simulation parameters were utilized (Table S1). Material parameters were assumed to be independent of temperature, and the initial temperature was set at standard cell culture temperature (~37 °C). Heat transfer was modeled using the heat-conduction equation

$$\nabla \cdot k\nabla T + Q = \rho c \frac{\partial T}{\partial t} \quad (1)$$

where Q is the Joule heat generated per unit volume per unit time, T is the temperature, t is the time, ρ is the density, c is the

https://doi.org/10.1021/acsomega.2c00284
ACS Omega 2022, 7, 23075−23082

specific heat, and k is the thermal conductivity. Bias pulses with different amplitudes in the 1−5 V range were administered to the cell system. The pulse length was set at 2 μs.

2.6. In Vitro Electrothermal Study. Cell suspensions with a density of 2×10^3 cells was seeded into a glass substrate/ITO system (Latech). A cloning cylinder (Sigma) was utilized to confine the cells. The cells were cultured for 24 h to allow cell attachment to the glass surface. The cells were then incubated with the material for 24 h. The bias pulses were administered to the system at an energy density of 5.9 J/mL (5 kV/cm, 2 μs, and 0.59 A/cm^2 pulses; 1000 pulses). The CV assay was utilized 24 h after the electrothermal experiment to measure cell viability.

3. RESULTS

3.1. Characterization of WS_2/PEG Nanostructures and Electrothermal Characterizations. Ultrasonication of bulk WS_2 yielded WS_2 nanostructures. We further synthesized WS_2 nanostructures with PEG for enhancing the stability of the nanostructure state and, at the same time, maintaining excellent biocompatibility. Raman spectroscopy was utilized to characterize the structure of WS_2. Experiments have demonstrated two Raman peaks around 400 cm^{-1}, which are called the $E_{2g}1$ and A_{1g} peaks.[19] Figure 2a and Supporting Information Figure S1

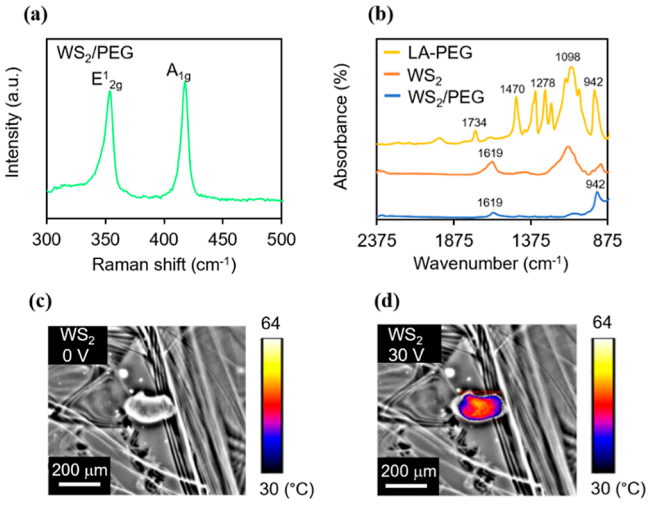

Figure 2. Characterization of WS_2/PEG nanostructures and electrothermal characterizations for AC-pulse ETT applications. (a) Raman spectra of WS_2/PEG. (b) FTIR spectra of LA-PEG, WS_2, and WS_2/PEG. (c,d) Thermal distributions of WS_2 at bias voltages of (c) 0 and (d) 30 V. The thermal signal images are superimposed on the optical images to mark the heating points with thermal data.

disclose the Raman spectra of pure WS_2 and WS_2/PEG nanostructures, and both the $E_{2g}1$ and A_{1g} peaks are present. The positions of the peaks were almost unchanged in the WS_2/PEG nanostructures, which indicate that the intrinsic structure of WS_2 was not affected by PEG. Moreover, to investigate the grafting of PEG on WS_2 surfaces, FTIR spectroscopy was used. The FTIR spectrum of WS_2/PEG nanostructures discloses typical stretching vibration of the carbonyl group in PEG at ∼942 cm^{-1},[20,21] indicating the surface presence of PEG. Additionally, AFM was utilized to characterize the WS_2 nanostructures before and after PEGylation. An average diameter of ∼200 nm and an average thickness of ∼27 nm were exhibited by the pure WS_2 nanostructures (Supporting Information Figure S2). The average diameter of WS_2 decreased (from ∼200 to 190 nm) after coating with LA-PEG as the sonication process may partially break down the nanostructures. However, the PEGylated WS_2 exhibited an increased thickness (from ∼27 to 41 nm) due to the existence of PEG coatings. Besides, we investigated the conductance of WS_2, WS_2/PEG, and PEG in DMEM. The WS_2/PEG samples showed a larger conductance compared to that of pure PEG samples (Supporting Information Figure S3) because PEG is an insulator. This indicates that WS_2 could efficiently convert electrical energy into thermal energy via Joule heating. Furthermore, the thermal distributions of WS_2 sheets upon the application of electrical stimuli were examined. As shown in Figure 2c,d, the peak temperature increases with an increase in stimulus amplitude, which can modulate the degree of ablation in cancer cells.

3.2. Biodegradation Behavior of WS_2/PEG Nanostructures. To understand the degradation behavior, we define the degree of degradation as the percentage decrease in absorbance {percentage decrease in absorbance = [(absorbance of the nanostructure after storage in a medium for specified time − absorbance of the pristine nanostructure)/absorbance of the pristine nanostructure] × 100%}. Thus, a larger percentage decrease in absorbance corresponds to a higher degree of degradation. Because we are interested in the variation of the degradation behavior of nanostructures, we record the variation of absorbance of nanostructures stored in DMEM for different nanostructures (Figure 3a,b, Supporting Information Figure S4). DMEM is a major component in cell media and is widely utilized to examine the stability of nanostructures in biological environments.[22] Thus, we chose to utilize DMEM as a medium to examine the biodegradation behavior. A clear dependence of the normalized absorbance on the storage time can be observed in Figure 3a,b and Supporting Information Figure S4. When the pure WS_2 was stored in DMEM for a week, the normalized absorbance decreased by ∼21% (Supporting Information Figure S4). In other words, the pure WS_2 showed a high degree of degradation. However, the normalized absorbance remained almost the same with an increase in storage time due to a constant degree of degradation. This means that the nanostructures with a consistently high degree of degradation could be fully degraded. Moreover, a lower degree of degradation should result in a smaller percentage decrease in normalized absorbance for the case of WS_2/PEG stored in DMEM for a week (∼15%) (Figure 3a,b). Additionally, the onset time of decrease in the normalized absorbance of WS_2/PEG kept in DMEM is ∼1 week, which is below the average of ∼3.5 weeks for state-of-the-art nanostructure-based systems in physiological media (Supporting Information Figure S5). Furthermore, it is likely that PEG isolates the interior WS_2 from DMEM, resulting in a low degree of degradation. PEG would then degrade via hydrolysis processes since DMEM is an aqueous medium.[23]

Moreover, XPS was utilized to investigate the interaction details between WS_2/PEG and DMEM. In the S 2p spectrum of pristine WS_2/PEG, the strong peak centered at ∼163 eV is attributed to the S $2p_{1/2}$ of S−S bonds.[24] For the WS_2/PEG stored in DMEM for a week, a similar peak was observed (Figure 3c). Another broad peak appeared at ∼169 eV, which was caused by the unavoidable oxidation of WS_2 to S_xO_y species.[25] The W 4f XPS spectrum was further analyzed (Supporting Information Figure S6). The WS_2/PEG after storage in DMEM for a week shows a strong peak at ∼31 eV corresponding to the W $4f_{7/2}$ of

https://doi.org/10.1021/acsomega.2c00284
ACS Omega 2022, 7, 23075−23082

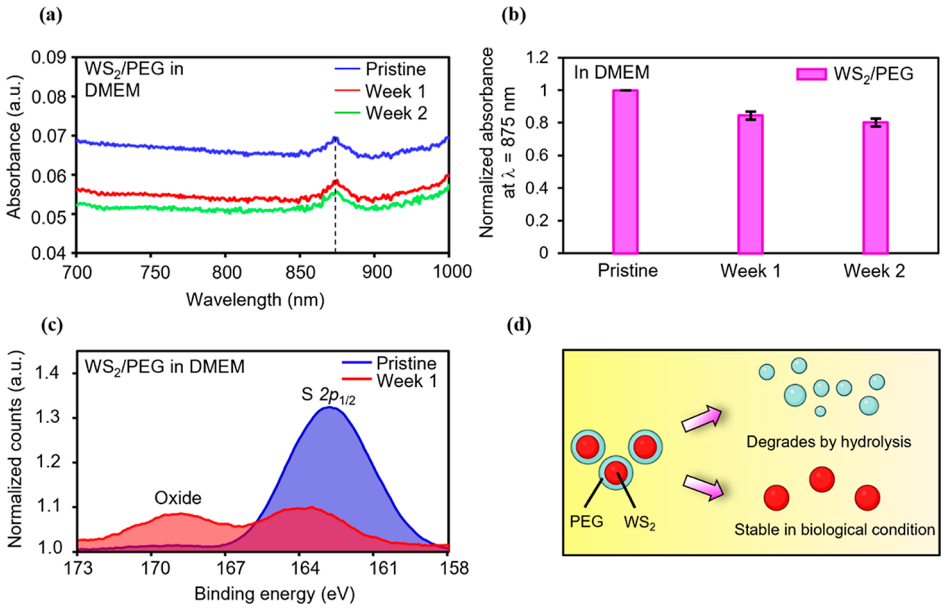

Figure 3. Biodegradation performance of WS_2/PEG nanostructures in DMEM for AC-pulse electrothermal therapeutics. (a) Absorbance spectra of the WS_2/PEG stored in DMEM for different weeks. (b) Variation of the normalized absorbance at a wavelength of 875 nm in different weeks. (c) XPS spectra showing the binding energies of S 2p of the pure WS_2 and WS_2/PEG stored in DMEM for a week. The XPS counts were normalized to background. (d) Schematic illustration of the biodegradation process of WS_2/PEG via a PEG-facilitated disrupt-and-release process in physiological environments.

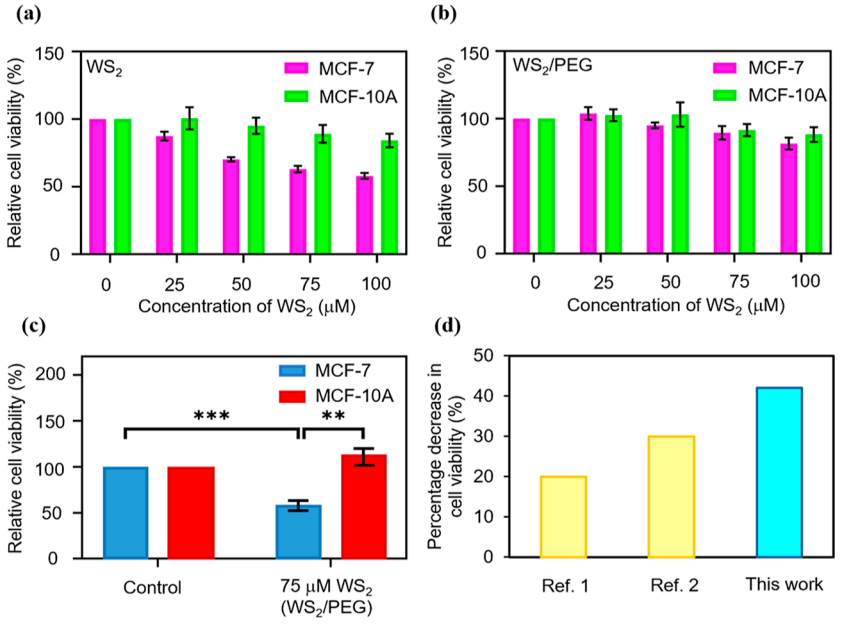

Figure 4. Combined effects of the AC pulse and WS_2/PEG nanostructure on ablating cancer cells. (a,b) Relative viability of the MCF-10A and MCF-7 cells after incubation with (a) pure WS_2 and (b) WS_2/PEG nanostructures for 24 h. The statistical significance of relative cell viabilities can be found in Supporting Information Table S2. (c) Relative viability of the MCF-10A and MCF-7 cells after incubation with WS_2/PEG nanostructures for 24 h and upon applying bias pulses. The control is defined as cells only after the application of bias pulses. Cell viability measurement was performed using the CV staining assay for (a−c), and the error bars represent SEM from three independent experiments ($n = 6$). Statistical significance was calculated based on the Student's *t*-test and is indicated as ** ($p < 0.01$) and *** ($p < 0.001$). (d) Comparison of the percentage decrease in cell viability of the MCF-7 cells with WS_2/PEG with that of the state-of-the-art electrothermal-based therapeutic system using similar energy densities. The information of the reference can be found in Supporting Information Table S3.

W^{4+}, which is typical of a WS_2 bond.[26] These results indicate that the oxidation can occur at the S site rather than at the W site.

The schematic illustration of the biodegradation process is shown in Figure 3d. Under physiological conditions, the external PEG shells degrade gradually due to the hydrolysis of ester linkage into smaller segments and monomers.[27] The degradation of PEG disrupts the nanostructures and triggers the release of interior WS_2 nanosheets.[28] Thus, the unique biodegradability of WS_2/PEG nanostructures enables increased stability of the nanostructure state and, at the same time, maintains excellent biocompatibility/biodegradability.

https://doi.org/10.1021/acsomega.2c00284
ACS Omega 2022, 7, 23075−23082

3.3. In Vitro Cytotoxicity Assays and AC-Pulse WS_2/PEG-Nanostructure-Based Electrothermal Experiments.

The cytotoxicity of the pure WS_2 and WS_2/PEG nanostructures in non-malignant breast epithelial cells (MCF-10A) and breast cancer cells (MCF-7) was investigated. The relative viability of both cell lines incubated with the nanostructures for ∼24 h was determined using the CV staining assay (Figure 4a,b). We observed that the cell viability of MCF-10A cells with pure WS_2 nanostructures decreases with an increase in WS_2 concentration. Moreover, the cell viability of MCF-10A cells with pure WS_2 nanostructures was higher than that of MCF-7 cells with WS_2 nanostructures (Figure 4a). For the MCF-10A cells with WS_2/PEG nanostructures, when an increased WS_2 concentration was utilized (0−100 μM), negligible cytotoxicity was observed (Figure 4b). However, for the MCF-7 cells with WS_2/PEG nanostructures, the cells disclosed an onset of a slight decrease in relative cell viability at ∼50−75 μM WS_2. Based on the cell viability constraints of MCF-7 and to achieve a high electrical conduction, we chose to utilize the WS_2/PEG nanostructures with 75 μM WS_2 for the ablation experiments.

The electrothermal ability of AC-pulse systems with WS_2/PEG nanostructures for ablating cancer cells was investigated. After ∼24 h of incubation with WS_2/PEG nanostructures, MCF-7 cells were injected with bias pulses, and the cell viability was assessed using the CV assay (Figure 4c). A low cell viability was observed for the MCF-7 cells with WS_2/PEG nanostructures (∼75 μM WS_2) upon the application of bias pulses. On the other hand, the application of bias pulses to the control (MCF-7 cells only) does not compromise cell viability. Moreover, we investigated the cell viability of MCF-10A cells under similar conditions. Both the control and MCF-10A cells with WS_2/PEG nanostructures (75 μM WS_2) showed excellent cell viability after applying bias pulses. The energy density of the system is estimated to be ∼5.9 J/mL (energy density = $n \times E \times j \times t$, where n is the number of pulses, E is the electric field, j is the current density, and t is the pulse length). Additionally, the MCF-7 cells with WS_2/PEG nanostructures showed a decrease in cell viability of ∼42%, above an average of ∼25% for current electrothermal-based therapeutic methods using similar energy densities (Figure 4d). These results demonstrate excellent electrothermal efficiency of WS_2/PEG nanostructures to specifically ablate cancer cells. Moreover, the incubation time of MCF-7 cells with WS_2/PEG nanostructures reached ∼24 h, which is above the average of ∼4.5 h for existing electrothermal-based therapeutic methods and with the use of the amount of time harnessed to incubate the cells with nanostructures prior to application of a stimulus as a measure of incubation time (Supporting Information Figure S7).

Besides, thermal distributions of the AC-pulse system with WS_2/PEG nanostructures were investigated using electrothermal simulations (Supporting Information Figure S8). When a bias pulse was injected (5 V, 2 μs), the model showed a large peak temperature (∼42.5 °C) in the cell layer, indicating that Joule heating of WS_2/PEG nanostructures could be propagated to neighboring cells. Based on this finding, we hypothesize that cell death may occur in MCF-7 cells with WS_2/PEG nanostructures upon the application of bias pulses due to strong Joule heating. In addition, simulations were performed to determine the electrical parameters utilized for in vitro experiments. The models disclosed that 5 V pulses were sufficient to ablate cancer cells and that rectangular pulses result in extended heating times (Supporting Information Figure S9). Moreover, the upper bound of bias generated by the pulse generator is 5 V. Based on these results and specifications and to attain a moderate ablation bias, rectangular pulses with an amplitude of 5 V were chosen for the experiments in vitro.

4. DISCUSSION

Traditional thermal-based ablation methods utilize a variety of energy sources (e.g., light irradiation and magnetic field) that are converted to heat, but their effectiveness can be compromised by insufficient depth of penetration into tissues.[29] Conventional photothermal-based ablation methodologies harness NIR light with a wavelength of 808 nm, which allows a penetration depth of 1−2 mm through tissues.[30] However, the amount of heat generated in deeper tissues (outside the irradiation area) tends to be limited. Emerging approaches, such as magnetic−thermal-based strategies, have also been investigated. The in vitro and in vivo experiments have demonstrated that AC magnetic field can achieve a deeper tissue penetration.[31,32] However, there is a limited number of techniques that can ablate cancer cells in vitro with high efficiency and using a short exposure time. Electrothermal ablation protocols can ablate cancer cells without affecting surrounding healthy cells. In this work, we demonstrate an electrothermal procedure that exhibits a short degradation time with an extended incubation period and a high ablation efficiency. We were able to achieve a decrease in cell viability of ∼42% for MCF-7 cells with WS_2/PEG nanostructures, which is above the average of ∼25% for current electrothermal-based therapeutic methods using similar energy densities. This enables the ablation of a larger population of cancer cells for enhancing treatment efficacy. Moreover, a degradation time of WS_2 of ∼1 week was realized, which is below the average of ∼3.5 weeks for current nanostructure-based systems in physiological media. This will permit the discharge of nanostructures from the body in a reasonable time for facilitating treatment safety. Furthermore, the incubation time of MCF-7 cells with WS_2/PEG nanostructures reached ∼24 h, which is above the average of ∼4.5 h for existing electrothermal-based therapeutic methodologies and with the use of the amount of time harnessed to incubate the cells with nanostructures prior to applying a stimulus as a measure of incubation time. This would allow the ablation of cancer cells with a longer time window for improving treatment efficacy.

Tungsten disulfide is an attractive electrothermal agent because it has excellent thermoelectric properties.[33] Moreover, its properties can be tuned by functionalization to improve, for example, cytotoxicity and degradability, since there are many active sites on the surface.[34] In this study, an improved material state of WS_2 was developed by surface modification with PEG. Compared with traditional thermal agents such as few-layered black phosphorous and gold nanoparticles,[7,35] WS_2/PEG nanostructures are attractive because of their unique biodegradability. PEG, which is FDA-approved, degrades by hydrolysis within a reasonable timeframe.[16] Upon administration into the body, the WS_2/PEG nanostructures can show increased circulation time and ensure sufficient tumor accumulation for highly efficient thermal-based cancer therapy.[36] The WS_2/PEG nanostructures can be utilized for an extended time without compromising their stability.[28] After fulfilling their therapeutic functions, the degradation of PEG can result in the release of WS_2. Although the investigation of the biodistribution of WS_2 is beyond the scope of this study, experiments have indicated that WS_2 can be uniformly distributed in tumor sites.[14] The accumulation occurs within 24 h after injection of WS_2/PEG in nude mice bearing MCF-7 and the nanostructures remain in

https://doi.org/10.1021/acsomega.2c00284
ACS Omega 2022, 7, 23075−23082

tumors for up to 120 h.[14] Furthermore, Hao et al. demonstrated that WS_2 was harmlessly excreted via the liver after 30 days.[28]

The studies for understanding nanostructure internalization within healthy and cancer cells have been reported previously.[14,37−40] For example, Duo et al. demonstrated cellular uptakes of molybdenum disulfide (MoS_2) nanosheets with PEG within the MCF-7 and MCF-10A cells.[39] The results suggested that the uptake was significantly higher in MCF-7 cells than in MCF-10A cells. In another experiment, Kong et al. disclosed similar results on the accumulation of PEGylated WS_2 structures in cancer cells.[14,40] It was suggested that the internalization had occurred via the endocytosis pathway.

Furthermore, it has been reported that nano−biointeractions between nanomaterials and cells can affect cell morphology. For instance, studies have reported that cells with PEG-coated nanomaterials are generally smooth and circular in appearance.[41,42] Bhattacharya et al. investigated the morphology of cancer cells (MCF-7) and healthy cells (HBL-100) with nanoparticles/PEG.[42] The cells were stained with Phalloidin and counter-stained with DAPI. Smooth surfaces and spherical shapes were shown by both cell lines, and the cells showed negligible cell damage. On the other hand, experiments have demonstrated that cancer cells with traditional pristine nanostructures may disclose physical damage.[43−45] Scanning electron microscopy (SEM) was utilized to characterize changes in the cellular morphology of MCF-7, liver cancer (HepG2), and cervical cancer (CaSki) cells with pure zinc oxide (ZnO) nanowires.[43] The SEM images show that these cells with ZnO nanowires may exhibit mechanical damage due to the disruption of the cell structure induced by one-dimensional nanomaterials and a large degree of change in cell morphology.[43] Therefore, further investigations may include morphological change of cells upon interaction with nanostructures.

5. CONCLUSIONS

These large decreases in cell viability for MCF-7 cells after AC pulse stimulation and excellent biodegradability are achieved through a PEG-facilitated disrupt-and-release process in electrothermal therapeutic systems that alters the biodegradation process of WS_2/PEG nanostructures. Furthermore, the proposed cancer therapy represents the first methodology reported using WS_2/PEG nanostructures for clinically relevant electrothermal cancer cell ablation and constitutes an extraordinary opportunity for the development of cancer treatment platforms.

■ ASSOCIATED CONTENT

Supporting Information

The Supporting Information is available free of charge at https://pubs.acs.org/doi/10.1021/acsomega.2c00284.

Properties utilized for simulation; statistical significance; list of references for comparison of percentage decrease in cell viability, degradation time and incubation time; Raman spectra of WS_2; AFM images of WS_2 and WS_2/PEG; conductance of WS_2, WS_2/PEG, and PEG; absorbance spectra of WS_2 before and after degradation; comparison of degradation time; XPS spectra after degradation; comparison of incubation time; and electrothermal simulation results (PDF)

■ AUTHOR INFORMATION

Corresponding Authors

Natasa Bajalovic − *Department of Science, Mathematics, and Technology, Singapore University of Technology and Design, Singapore 487372, Singapore*; Email: natasa_bajalovic@sutd.edu.sg

Desmond K. Loke − *Department of Science, Mathematics, and Technology, Singapore University of Technology and Design, Singapore 487372, Singapore; Office of Innovation, Changi General Hospital, Singapore 529889, Singapore*; orcid.org/0000-0001-5799-6441; Email: desmond_loke@sutd.edu.sg

Authors

Maria Prisca Meivita − *Department of Science, Mathematics, and Technology, Singapore University of Technology and Design, Singapore 487372, Singapore*; orcid.org/0000-0003-1518-0772

Sophia S. Y. Chan − *Department of Science, Mathematics, and Technology, Singapore University of Technology and Design, Singapore 487372, Singapore*; orcid.org/0000-0001-6710-0469

Shao Xiang Go − *Department of Science, Mathematics, and Technology, Singapore University of Technology and Design, Singapore 487372, Singapore*

Denise Lee − *Department of Science, Mathematics, and Technology, Singapore University of Technology and Design, Singapore 487372, Singapore*; orcid.org/0000-0001-5338-275X

Complete contact information is available at: https://pubs.acs.org/10.1021/acsomega.2c00284

Notes

The authors declare no competing financial interest.

■ ACKNOWLEDGMENTS

We thank W.C. Teoh (Changi General Hospital, Singapore), K.G. Lim, L.T. Ng, A.H. Firdaus, and J.Y. Koh for support and important discussions. The authors acknowledge support from the Ministry of Education (Singapore) (MOE-T2EP50220-0022), Changi General Hospital (Singapore) (CGH-SUTD-HTIF2019-001), and SUTD-Zhejiang-University (SUTD-ZJU (VP) 201903) grant programs. D.K.L. acknowledges support from the Massachusetts Institute of Technology−SUTD International Design Centre and National Supercomputing Centre, Singapore (15001618). M.P.M. acknowledges support from the SUTD President Graduate Scholarship.

■ REFERENCES

(1) Cancer Statistics-National Cancer Institute. https://www.cancer.gov/about-cancer/understanding/statistics (accessed Sep 2021, 30).

(2) Sung, H.; Ferlay, J.; Siegel, R. L.; Laversanne, M.; Soerjomataram, I.; Jemal, A.; Bray, F. Global Cancer Statistics 2020: GLOBOCAN Estimates of Incidence and Mortality Worldwide for 36 Cancers in 185 Countries. *Ca-Cancer J. Clin.* **2021**, *71*, 209−249.

(3) Long COVID Appears to "Impair" Survival in Cancer Patients http://www.medscape.com/viewarticle/959251 (accessed Oct 2021, 25).

(4) van der Zee, J. Heating the Patient: A Promising Approach? *Ann. Oncol.* **2002**, *13*, 1173−1184.

(5) Huang, X.; Neretina, S.; El-Sayed, M. A. Gold Nanorods: From Synthesis and Properties to Biological and Biomedical Applications. *Adv. Mater.* **2009**, *21*, 4880−4910.

(6) Kumar, S.; Hasumura, T.; Nagaoka, Y.; Yoshida, Y.; Maekawa, T.; Jeymohan, P. Accelerated Killing of Cancer Cells Using a Multifunctional Single-Walled Carbon Nanotube-Based System for Targeted Drug Delivery in Combination with Photothermal Therapy. *Int. J. Nanomed.* **2013**, *8*, 2653−2667.
(7) Li, L.; Belcher, A. M.; Loke, D. K. Simulating selective binding of a biological template to a nanoscale architecture: a core concept of a clamp-based binding-pocket-favored N-terminal-domain assembly. *Nanoscale* **2020**, *12*, 24214−24227.
(8) Golombek, S. K.; May, J.-N.; Theek, B.; Appold, L.; Drude, N.; Kiessling, F.; Lammers, T. Tumor Targeting via EPR: Strategies to Enhance Patient Responses. *Adv. Drug Delivery Rev.* **2018**, *130*, 17−38.
(9) Yong, Y.; Zhou, L.; Gu, Z.; Yan, L.; Tian, G.; Zheng, X.; Liu, X.; Zhang, X.; Shi, J.; Cong, W.; Yin, W.; Zhao, Y. WS_2 Nanosheet as a New Photosensitizer Carrier for Combined Photodynamic and Photothermal Therapy of Cancer Cells. *Nanoscale* **2014**, *6*, 10394−10403.
(10) Liao, W.; Zhang, L.; Zhong, Y.; Shen, Y.; Li, C.; An, N. Fabrication of Ultrasmall WS_2 Quantum Dots-Coated Periodic Mesoporous Organosilica Nanoparticles for Intracellular Drug Delivery and Synergistic Chemo-Photothermal Therapy. *OncoTargets Ther.* **2018**, *11*, 1949−1960.
(11) Loke, D. K.; Clausen, G. J.; Ohmura, J. F.; Chong, T.-C.; Belcher, A. M. Biological-templating of a segregating binary alloy for nanowire-like phase-change materials and memory. *ACS Appl. Nano Mater.* **2018**, *1*, 6556−6562.
(12) Wang, Q. H.; Kalantar-Zadeh, K.; Kis, A.; Coleman, J. N.; Strano, M. S. Electronics and Optoelectronics of Two-Dimensional Transition Metal Dichalcogenides. *Nat. Nanotechnol.* **2012**, *7*, 699−712.
(13) Gusakova, J.; Wang, X.; Shiau, L. L.; Krivosheeva, A.; Shaposhnikov, V.; Borisenko, V.; Gusakov, V.; Tay, B. K. Electronic Properties of Bulk and Monolayer TMDs: Theoretical Study Within DFT Framework (GVJ-2e Method). *Phys. Status Solidi A* **2017**, *214*, 1700218.
(14) Kong, N.; Ding, L.; Zeng, X.; Wang, J.; Li, W.; Shi, S.; Gan, S. T.; Zhu, X.; Tao, W.; Ji, X. Comprehensive Insights into Intracellular Fate of WS_2 Nanosheets for Enhanced Photothermal Therapeutic Outcomes via Exocytosis Inhibition. *Nanophotonics* **2019**, *8*, 2331−2346.
(15) Yi, H.; Zhou, X.; Zhou, C.; Yang, Q.; Jia, N. Liquid Exfoliated Biocompatible WS_2@BSA Nanosheets with Enhanced Theranostic Capacity. *Biomater. Sci.* **2021**, *9*, 148−156.
(16) Suk, J. S.; Xu, Q.; Kim, N.; Hanes, J.; Ensign, L. M. PEGylation as a Strategy for Improving Nanoparticle-Based Drug and Gene Delivery. *Adv. Drug Delivery Rev.* **2016**, *99*, 28−51.
(17) Jokerst, J. V.; Lobovkina, T.; Zare, R. N.; Gambhir, S. S. Nanoparticle PEGylation for Imaging and Therapy. *Nanomed* **2011**, *6*, 715−728.
(18) Feng, W.; Chen, L.; Qin, M.; Zhou, X.; Zhang, Q.; Miao, Y.; Qiu, K.; Zhang, Y.; He, C. Flower-like PEGylated MoS_2 Nanoflakes for near-Infrared Photothermal Cancer Therapy. *Sci. Rep.* **2015**, *5*, 17422.
(19) Perea-López, N.; Elías, A. L.; Berkdemir, A.; Castro-Beltran, A.; Gutiérrez, H. R.; Feng, S.; Lv, R.; Hayashi, T.; López-Urías, F.; Ghosh, S.; Muchharla, B.; Talapatra, S.; Terrones, H.; Terrones, M. Photosensor Device Based on Few-Layered WS_2 Films. *Adv. Funct. Mater.* **2013**, *23*, 5511−5517.
(20) Khanna, L.; Verma, N. K. PEG/$CaFe_2O_4$ Nanocomposite: Structural, Morphological, Magnetic and Thermal Analyses. *Phys. Rev. B: Condens. Matter Mater. Phys.* **2013**, *427*, 68−75.
(21) Olmo, C.; Franco, L.; del Valle, L. J.; Puiggalí, J. Biodegradable Polylactide Scaffolds with Pharmacological Activity by Means of Ultrasound Micromolding Technology. *Appl. Sci.* **2020**, *10*, 3106.
(22) Guerrini, L.; Alvarez-Puebla, R.; Pazos-Perez, N. Surface Modifications of Nanoparticles for Stability in Biological Fluids. *Materials* **2018**, *11*, 1154.
(23) Visan, A. I.; Popescu-Pelin, G.; Socol, G. Degradation Behavior of Polymers Used as Coating Materials for Drug Delivery—A Basic Review. *Polymers* **2021**, *13*, 1272.
(24) Akhavan, B.; Jarvis, K.; Majewski, P. Development of Oxidized Sulfur Polymer Films through a Combination of Plasma Polymerization and Oxidative Plasma Treatment. *Langmuir* **2014**, *30*, 1444−1454.
(25) Ishida, T.; Choi, N.; Mizutani, W.; Tokumoto, H.; Kojima, I.; Azehara, H.; Hokari, H.; Akiba, U.; Fujihira, M. High-Resolution X-Ray Photoelectron Spectra of Organosulfur Monolayers on Au(111): S(2p) Spectral Dependence on Molecular Species. *Langmuir* **1999**, *15*, 6799−6806.
(26) Zabinski, J. S.; Donley, M. S.; Prasad, S. V.; McDevitt, N. T. Synthesis and Characterization of Tungsten Disulphide Films Grown by Pulsed-Laser Deposition. *J. Mater. Sci.* **1994**, *29*, 4834−4839.
(27) Hamidi, M.; Azadi, A.; Rafiei, P. Pharmacokinetic Consequences of Pegylation. *Drug Delivery* **2006**, *13*, 399−409.
(28) Hao, J.; Song, G.; Liu, T.; Yi, X.; Yang, K.; Cheng, L.; Liu, Z. In Vivo Long-Term Biodistribution, Excretion, and Toxicology of PEGylated Transition-Metal Dichalcogenides MS_2 (M = Mo, W, Ti) Nanosheets. *Adv. Sci.* **2016**, *4*, 1600160.
(29) Deng, X.; Shao, Z.; Zhao, Y. Solutions to the Drawbacks of Photothermal and Photodynamic Cancer Therapy. *Adv. Sci.* **2021**, *8*, 2002504.
(30) Algorri, J. F.; Ochoa, M.; Roldán-Varona, P.; Rodríguez-Cobo, L.; López-Higuera, J. M. Light Technology for Efficient and Effective Photodynamic Therapy: A Critical Review. *Cancers* **2021**, *13*, 3484.
(31) Lee, J.-H.; Jang, J.-t.; Choi, J.-s.; Moon, S. H.; Noh, S.-h.; Kim, J.-w.; Kim, J.-G.; Kim, I.-S.; Park, K. I.; Cheon, J. Exchange-Coupled Magnetic Nanoparticles for Efficient Heat Induction. *Nat. Nanotechnol.* **2011**, *6*, 418−422.
(32) Jordan, A.; Scholz, R.; Wust, P.; Schirra, H.; Schiestel, T.; Schmidt, H.; Felix, R. Endocytosis of Dextran and Silan-Coated Magnetite Nanoparticles and the Effect of Intracellular Hyperthermia on Human Mammary Carcinoma Cells in Vitro. *J. Magn. Magn. Mater.* **1999**, *194*, 185−196.
(33) Kandemir, A.; Yapicioglu, H.; Kinaci, A.; Çağın, T.; Sevik, C. Thermal Transport Properties of MoS_2 and $MoSe_2$ Monolayers. *Nanotechnology* **2016**, *27*, 055703.
(34) Chen, H.; Liu, T.; Su, Z.; Shang, L.; Wei, G. 2D Transition Metal Dichalcogenide Nanosheets for Photo/Thermo-Based Tumor Imaging and Therapy. *Nanoscale Horiz.* **2018**, *3*, 74−89.
(35) Vines, J. B.; Yoon, J.-H.; Ryu, N.-E.; Lim, D.-J.; Park, H. Gold Nanoparticles for Photothermal Cancer Therapy. *Front. Chem.* **2019**, *7*, 167.
(36) Cheng, L.; Liu, J.; Gu, X.; Gong, H.; Shi, X.; Liu, T.; Wang, C.; Wang, X.; Liu, G.; Xing, H.; Bu, W.; Sun, B.; Liu, Z. PEGylated WS_2 Nanosheets as a Multifunctional Theranostic Agent for in Vivo Dual-Modal CT/Photoacoustic Imaging Guided Photothermal Therapy. *Adv. Mater.* **2014**, *26*, 1886−1893.
(37) Zhang, Y.; Yang, M.; Portney, N.; Cui, D.; Budak, G.; Ozbay, E.; Ozkan, M.; Ozkan, C. Zeta Potential: A Surface Electrical Characteristic to Probe the Interaction of Nanoparticles with Normal and Cancer Human Breast Epithelial Cells. *Biomed. Microdevices* **2008**, *10*, 321−328.
(38) Calero, M.; Chiappi, M.; Lazaro-Carrillo, A.; Rodríguez, M. J.; Chichón, F. J.; Crosbie-Staunton, K.; Prina-Mello, A.; Volkov, Y.; Villanueva, A.; Carrascosa, J. L. Characterization of Interaction of Magnetic Nanoparticles with Breast Cancer Cells. *J. Nanobiotechnol.* **2015**, *13*, 16.
(39) Duo, Y.; Li, Y.; Chen, C.; Liu, B.; Wang, X.; Zeng, X.; Chen, H. DOX-Loaded PH-Sensitive Mesoporous Silica Nanoparticles Coated with PDA and PEG Induce pro-Death Autophagy in Breast Cancer. *RSC Adv.* **2017**, *7*, 39641−39650.
(40) Zhu, X.; Ji, X.; Kong, N.; Chen, Y.; Mahmoudi, M.; Xu, X.; Ding, L.; Tao, W.; Cai, T.; Li, Y.; Gan, T.; Barrett, A.; Bharwani, Z.; Chen, H.; Farokhzad, O. C. Intracellular Mechanistic Understanding of 2D MoS_2 Nanosheets for Anti-Exocytosis-Enhanced Synergistic Cancer Therapy. *ACS Nano* **2018**, *12*, 2922−2938.
(41) Mishra, S.; Webster, P.; Davis, M. E. PEGylation Significantly Affects Cellular Uptake and Intracellular Trafficking of Non-Viral Gene Delivery Particles. *Eur. J. Cell Biol.* **2004**, *83*, 97−111.
(42) Bhattacharya, S.; Ahir, M.; Patra, P.; Mukherjee, S.; Ghosh, S.; Mazumdar, M.; Chattopadhyay, S.; Das, T.; Chattopadhyay, D.; Adhikary, A. PEGylated-Thymoquinone-Nanoparticle Mediated Retardation of Breast Cancer Cell Migration by Deregulation of

https://doi.org/10.1021/acsomega.2c00284
ACS Omega 2022, 7, 23075−23082

Cytoskeletal Actin Polymerization through MiR-34a. *Biomaterials* **2015**, *51*, 91−107.
(43) Ning, R.; Wang, S.; Wu, J.; Wang, F.; Lin, J.-M. ZnO Nanowire Arrays Exhibit Cytotoxic Distinction to Cancer Cells with Different Surface Charge Density: Cytotoxicity Is Charge-Dependent. *Small* **2014**, *10*, 4113.
(44) Feng, W.; Nie, W.; Cheng, Y.; Zhou, X.; Chen, L.; Qiu, K.; Chen, Z.; Zhu, M.; He, C. In Vitro and in Vivo Toxicity Studies of Copper Sulfide Nanoplates for Potential Photothermal Applications. *Nanomedicine Nanotechnol. Biol. Med.* **2015**, *11*, 901−912.
(45) Mohammed, A. E.; Al-Megrin, W. A. Biological Potential of Silver Nanoparticles Mediated by Leucophyllum Frutescens and Russelia Equisetiformis Extracts. *Nanomater.* **2021**, *11*, 2098.

https://doi.org/10.1021/acsomega.2c00284
ACS Omega 2022, 7, 23075−23082